CHAPTER 2

Literature review

2.1 Crystalline structures, properties and applications of metal oxides

2.1.1 MoO_3

Basically, molybdenum oxides are classified into two types: the thermo-dynamically stable orthorhombic α-MoO_3 phase, and the metastable monoclinic β-MoO_3 phase with ReO_3-type structure. Orthorhombic α-MoO_3 phase is a promising oxide, with structural anisotropy [23]. Molybdenum oxide (MoO_3) powder has a white or light gray color. T. He [23] had described this structure which consists of corner-sharing chains of MoO_6 octahedral that share edges with two similar chains to form layers of MoO_3 stoichiometry. These layers are stacked in a staggered arrangement and are only held together by weak van der Waals forces (Figure 2.1 a). The type of molybdenum oxide of interest in this review has a monoclinic structure (β-phase), which is of the perovskite-like type (ReO_3 structure) and can be regarded as an infinite framework of corner-sharing MoO_6 octahedra, each with a central Mo atom surrounded by six almost equidistant oxygen atoms (figure 2.1 b and 2.1 c). In between these octahedra, there are extended tunnels that can serve as conduits and intercalation sites for mobile ions. The MoO_6 octahedron is the building block for both the orthorhombic and monoclinic structure.

Therefore, it is a wide band gap n-type semiconductor, which is very attractive for different technological applications such as photochromic materials (changing from colorless to blue by UV irradiation) [23-25], smart

windows [26], self-developing photography [23], conductive gas sensors [24], lubricants [27], and catalysts [28]. Some physical properties of MoO_3 are shown in Table 2.1.

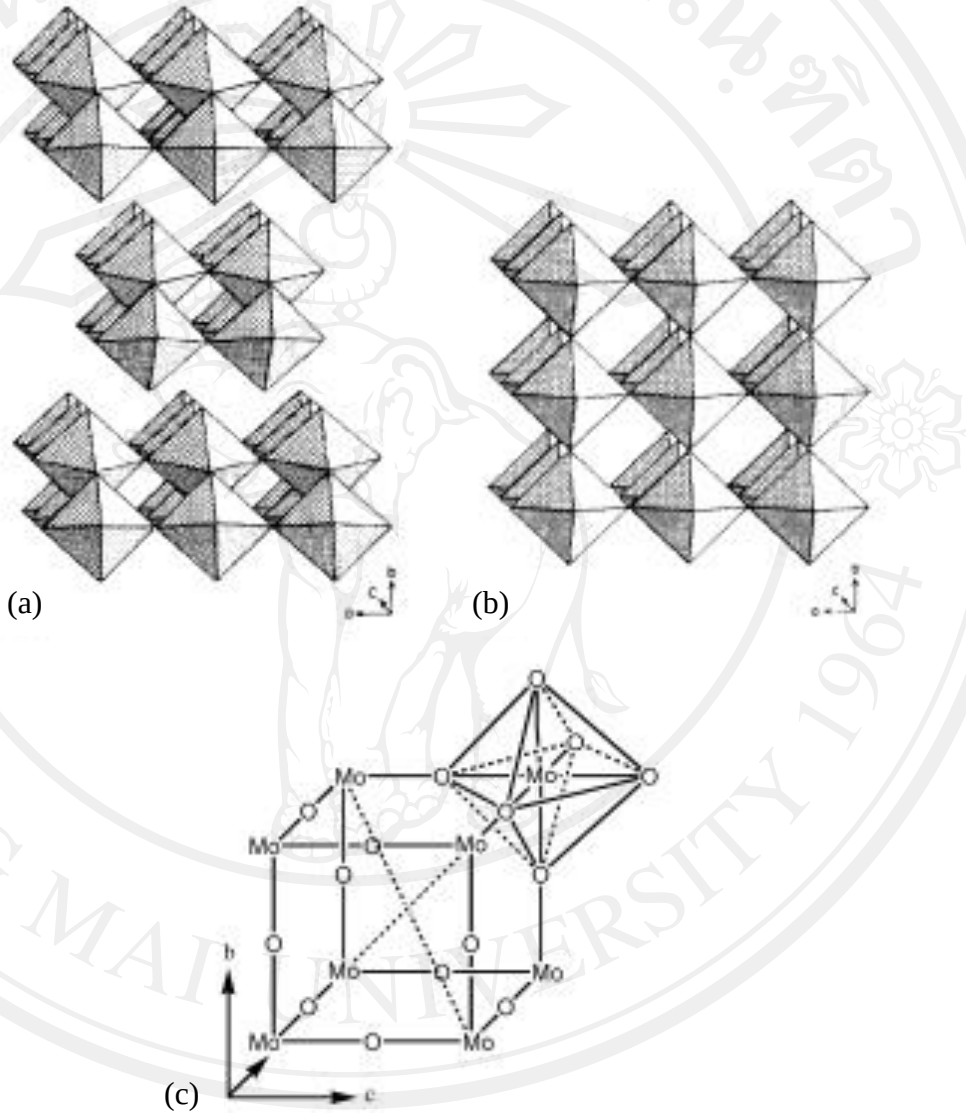

Figure 2.1 The structures [36] of (a) α-MoO_3, (b) ReO_3 and (c) unit cell for the lattice of ReO_3. The octahedral symmetry is emphasized in (c)

Table 2.1 some physical properties of MoO_3 [29]

properties	
Molecular formula	MoO_3
Molar mass	143.94 g mol^{-1}
Density	4.69 g/cm^3, solid
Melting point	795 °C
Boiling point	1155 °C
Solubility in water	0.1066 g/100 mL (18 °C) 2.055 g/100 mL (70 °C)

Thermal decomposition of $(NH_4)_6Mo_7O_{24}\cdot 4H_2O$ was studied in a several time. NH_3 and H_2O are given off when heat radiation performs. Intermediate phase of higher Mo content are formed when temperature slightly increase. A final product of MoO_3 exists under the condition of following mechanism[30,31]:

$$(NH_4)_6Mo_7O_{24}\cdot 4H_2O \xrightarrow{\sim 110^\circ C} (NH_4)_4Mo_5O_{17} + NH_3\uparrow + H_2O\uparrow \quad (2.1)$$

$$(NH_4)_4Mo_5O_{17} \xrightarrow{\sim 220^\circ C} (NH_4)_2Mo_4O_{13} + NH_3\uparrow + H_2O\uparrow \quad (2.2)$$

$$(NH_4)_2Mo_4O_{13} \xrightarrow{\sim 360^\circ C} MoO_3 + NH_3\uparrow + H_2O\uparrow \quad (2.3)$$

$$\beta\text{-}(NH_4)_2Mo_4O_{13} \xrightarrow{\sim 316-348^\circ C} MoO_3 + NH_3\uparrow + H_2O\uparrow \quad (2.4)$$

2.1.3 CuO

The original crystal structure of CuO was first determined by Tunnel in 1933 and was then refined by single-crystal X-ray methods in 1970 [32]. Contrary to the usual rock-salt structure of other 3d transition-metal monoxides, the CuO crystal structure is monoclinic with C2/c symmetry and four formula units per unit cell. The Cu2+ ions are at centers of inversion symmetry in a single fourfold site 4c (1/4, 1/4,0), and the oxygen ions occupy site 4e (0,y,1/4) with y = 0.416(2) (Figure 2.2) [33–36]. The structural parameters as summarized by Meyer et al. [36] are listed in Table 2.2.

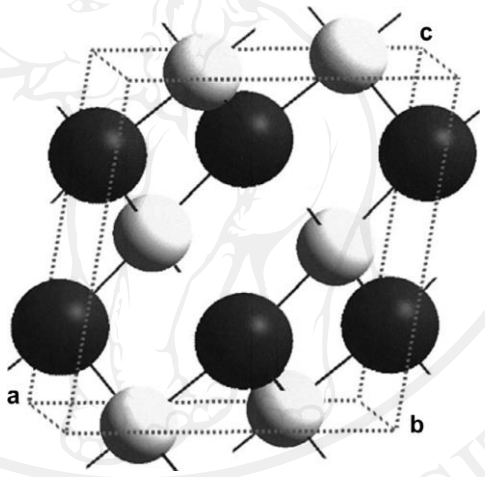

Figure 2.2 Crystal structure of CuO (tenorite). The special atomic positions for Cu are (1/4, 1/4, 0), (3/4, 3/4, 0), (1/4, 3/4, 1/2), and (3/4, 1/4,1/2) and for oxygen are (0,y, 1/4), (0,1/2 + y, 1/4), (0, -y, 3/4), and (1/2,-1/2 y,3/4) with y = 0.416. The small light spheres and large dark spheres represent Cu and oxygen atoms, respectively [35].

Table 2.2 Structural parameters of CuO [36]

Space group	C 2/c (No.15)
Unit cell	a (A˚) = 4.6837 b (A˚) = 3.4226 c (A˚) = 5.1288 β (θ) = 99.54 α (θ) = 90
Cell volume	81.08 A
Cell content	4 [CuO]
Formula weight	79.57
Distances	Cu–O, 1.96 A˚ O–O, 2.62 A˚ Cu–Cu, 2.90 A˚

Table 2.3 Key physical properties of CuO at room temperature (300 K)[37]

Density	6.31 g/cm^3
Melting point	1200 ˚C
Stable phase at 300 K	Monoclinic
Dielectric constant	18.1
Refractive index	1.4
Bang gap (Eg)	1.21–1.55 eV direct
Hole effective mass	0.24 mo
Hole mobility	0.1–10 cm^2/V s

In application, the recent developments in the different CuO nanostructures as building blocks for applications in a wide range of fields. These fields include supercapacitors, sensors, solar cells, photodetectors, catalysis, nanofluid, nanoenergetic materials (nEMs), field emissions, superhydrophobic surfaces, and removal of arsenic and organic pollutants from waste water.

Among various MOS, CuO has the unique property of being intrinsically p-type and is advantageous because of its low cost, high stability, nontoxicity, and capability for electron transfer [38]. Therefore, CuO nanostructures have been extensively investigated as good candidates for sensing applications. Gas sensors based on CuO nanostructures were

operated by measuring the resistance changes when they are exposed to reducing or oxidizing gases [39]. A suitable operation temperature is crucial to the gas sensing capability of CuO because it enhances the sensitivity and reduces the response and recovery time[40]. Coating of noble metal catalysts, such as Ag, Au, Pd, and Pt, on the surface of CuO nanostructures will enhance their sensing properties because they can act as adsorption sites for analyses or as surface catalyst [40,41].

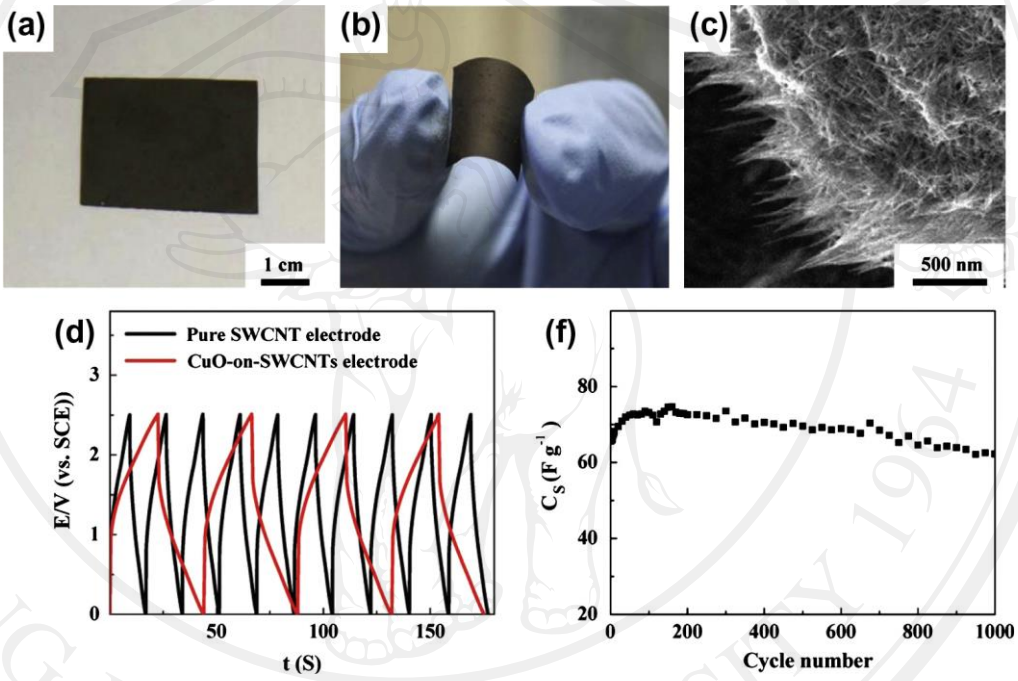

Figure 2.3 (a and b) Optical images of CuO nanobelt-based two-layered SWCNTs and CuO nanobelts mixed with SWCNT (9:1 weight ratio) electrode. (c) Edge of SWCNTs and CuO nanobelts. (d) Galvanostatic charge/discharge curves measured with a current density of 5 A/g for different electrodes. (e) Cycling performance for SWCNTs and CuO nanobelts mixed with SWCNT electrode at a current density of 5 A/g in 1.0 M LiPF6/EC: DEC [42].

2.2 Microwave synthesis

2.2.1 Introduction

Microwave are electromagnetic radiation (Figure 2.4) [43] composing of electric field and magnetic field, but only electric field can transfer energy to heat substance. For magnetic field, it was not reported. It's wavelengths measure in the range of around 1 mm to 1 m (frequency range of 300 MHz to 300 GHz) (Figure 2.5). For the microwave frequency, molecule rotation occurs only without molecular structure change. An applications of the microwave spectrum are used for point to point communication, TV broadcasting and RADAR. Beside these, they are also used in industrial, biomedical and in laboratory[44].

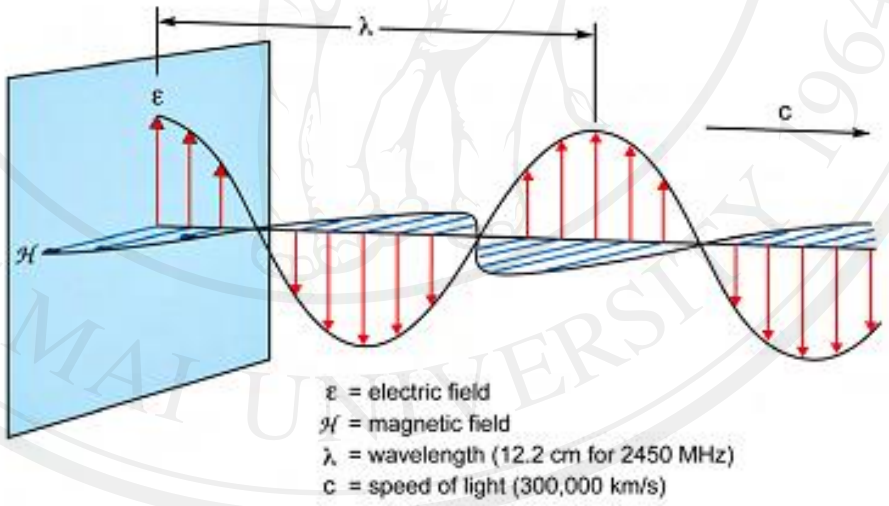

Figure 2.4 Composition of electromagnetic wave[43].

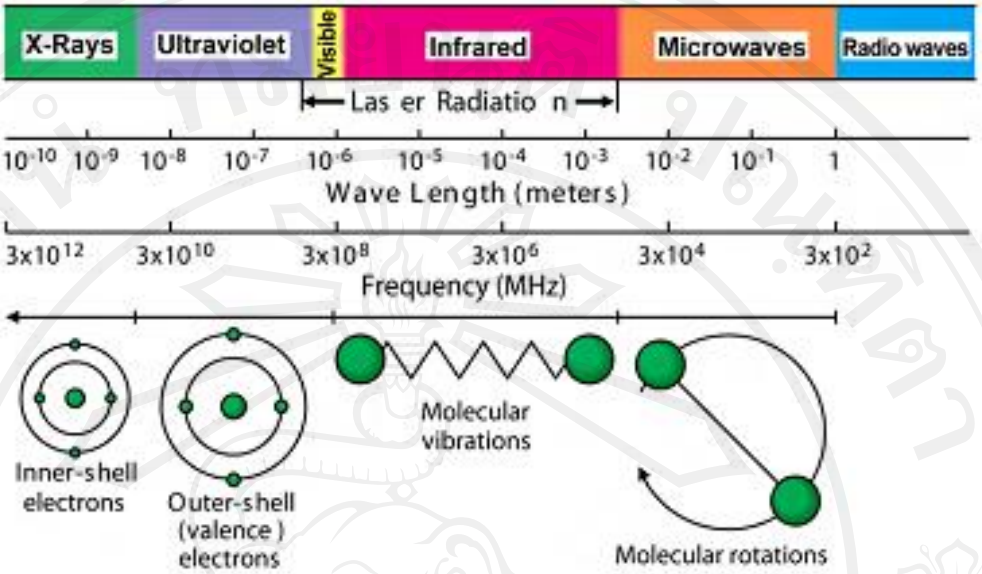

Figure 2.5 Electromagnetic spectrum and it's interaction with molecule[43]

Only frequency at 900 MHz and 2.45 GHz are allowed for microwave heating purposes. Other frequencies of microwave applications involving heating have been reported for 28, 30, 60, and 83 GHz have been used [45-48]. As is well-known, microwaves are produced by magnetrons. From the magnetrons, the microwaves are generally directed toward a target (placed in be called microwave cavities) with the use of microwave guides. These guides are usually made of sheet metal, and the intensity distribution within the waveguides is homogenized by the use of mode stirrers[47]. Many microwave preparations reported in the literature have been made on the laboratory scale of only a few grams. These preparations have all been made with the use of domestic microwave ovens operating at 2.45GHz and with a maximum output power of 1 kW. However, use of higher power levels for specialized applications have also been reported[46-48].

2.2.2 Microwave heating

1). **Microwave versus conventional heating** Microwave and conventional processing have a different heating mechanism. E.T. Thostenson [49] has explained that conventional heating, energy is transferred to the material through convection, conduction, and radiation of heat from the surfaces of the material. For microwave heating, energy is delivered directly to materials through molecular interaction with the electromagnetic field. In heat transfer, energy is transferred due to thermal gradients, but microwave heating is the transfer of electromagnetic energy to thermal energy, rather than heat transfer (Figure 2.6). For this difference, energy is delivered can result in many potential advantages to using microwaves for processing of materials, due to microwaves can penetrate in materials and deposit energy. Heat can be generated throughout the volume of the material. The transfer of energy does not rely on diffusion of heat from the surfaces, and it is possible to achieve rapid and uniform heating of thick materials. In traditional heating, the cycle time is often dominated by slow heating rates that are chosen to minimize steep thermal gradients that result in process-induced stresses. For polymers and ceramics, these materials have a low thermal conductivities, this can result in significantly reduced processing times. Thus, there often is a balance between processing time and product quality in conventional processing. As microwaves can transfer energy throughout the volume of the material, the potential exists to reduce processing time and enhance overall quality.

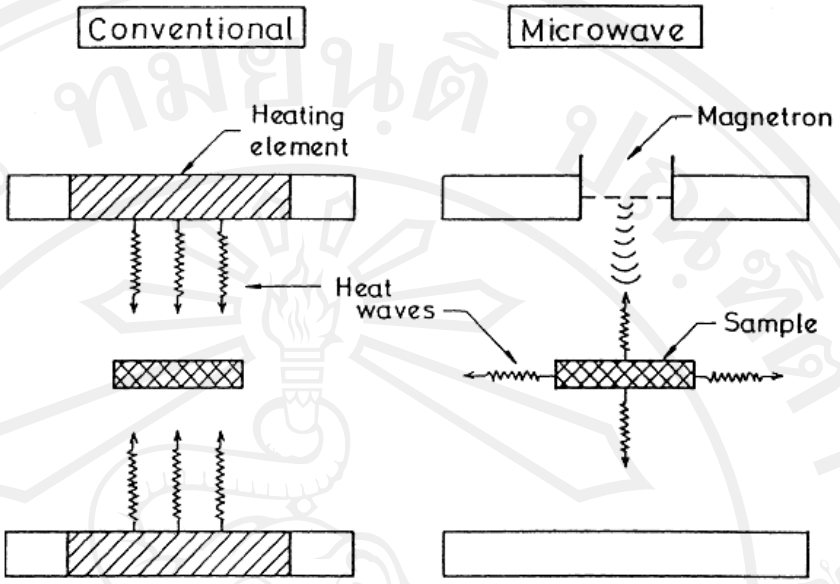

Figure 2.6 comparison heating mechanism between conventional and microwave oven [50].

2). Interaction of microwaves with materials

There are two important factors to select the frequency of microwave radiation to heat the materials[51]: (1) power absorption in the matter, and (2) depth of penetration. In electromagnetism, materials are divided into two types: (1) conductors and (2) insulators or dielectrics. The distinction between them is not very sharp.The same material may behave as a conductor in one part of electromagnetic frequency and as a dielectric in another. According to Maxwell's theory, the ratio of $(\sigma / \omega\varepsilon)$ is considered to be a dividing factor where σ is the electrical conductivity; ω is the angular frequency and ε is the permittivity/ dielectric constant. For good conductor, this ratio is much greater than unity while in dielectrics, it is much smaller than unity. For dielectrics, the electrostatic fields can persist for a long time offering very high resistance when static voltage is applied whereas in

good conductors (metals) the static current feels negligible resistance. At higher frequencies, the behavior depends upon frequency of the electromagnetic waves and corresponding conductivity, permittivity, permeability of the material. The electromagnetic energy propagation through a material medium is associated with the numerical values of permittivity or dielectric constant at that frequency. The absorption of electromagnetic energy depends upon complex permittivity ε of that material and can be expressed as

$$\varepsilon = \varepsilon' + i\varepsilon'' \qquad (2.5)$$

where ε' = the real component of permittivity

ε'' = the imaginary component of permittivity

The real part or relative permittivity represents the degree to which an electric field may built up inside a material when exposed to the electric field while the imaginary part or dielectric loss is a measure of amount of the field transformed into heat. The Loss angle δ, the phase difference between the electric field and the polarization of the material is related to the complex dielectric constant as

$$tan\delta = \varepsilon''/\varepsilon' \qquad (2.6)$$

Thus the tan δ, the dissipation factor determines the ability of material to transform absorbed energy into heat.

In terms of microwave interaction, the materials can be classified into three categories:

2.1) Microwave reflectors e.g. metals

2.2) Microwave transmitters – transparent to microwave radiations e.g. fused quartz, ceramics, zircon etc.; tan $\delta < 0.1$

2.3) Microwave absorbers taking up energy from the microwave field and heating the materials rapidly; tan $\delta > 0.1$

The electromagnetic energy absorption in dielectric materials primarily is due to the existence of permanent dipole moment of the molecules which tend to orient and reorient under the influence of electric field of microwave. The reorientation loss mechanism originates from the inability of the polarization to follow extremely rapid reversals of the electric field. In the low frequency (up to 100 MHz) electric field, the dipoles easily follow the changes in the field and their orientation changes in phase with the field. At higher frequencies the inertia of molecules and their interactions with neighbours make changing orientation more difficult and the dipoles lag behind the field. As a result, the conduction current density has a component in phase with the field and therefore power is dissipated in the dielectric material. At very high frequencies (1- 10 THz), the molecules can no longer respond to the electric field. At GHz frequency (ideal working range) the phase lag of the dipoles behind the electric field absorbs power from the field and therefore pronounced as dielectric loss due to dipole relaxation.

Another important parameter for microwave heating ,penetration depth D_{ph} is defined as the depth into the material where the power is reduced to ~ 1/3 of the original intensity . The absorption coefficient α of dielectric material is related to imaginary parts of dielectric constant ε'' or the refractive index. The depth of penetration D_{ph} of electromagnetic waves in matter is related to α as $D_{ph} = 1/\alpha$.

Thus a material with higher dissipation factor will have lower penetration depth. The wavelength of the radiation also has influence on penetration depth. For microwave prone materials, the absorption coefficient at 2.45 GHz is moderate and depth of penetration is of the order of 10 cm to 1m which results in absorption of microwave everywhere in material. The intensity of heat evolution in a sample depends on electrophysical properties of the materials, frequency, intensity of the applied field, penetration depth of the electromagnetic waves into the substance under treatment and geometric size of the sample. The dielectric parameter of the matter and the penetration depth depend strongly on temperature and therefore varies during heating. Water is an excellent example of polar molecule. The principle of microwave heating of polar molecules (for the case of water) is illustrated very nicely in figure 2.7 [52]. These molecules absorb microwave energy rapidly and the rate of absorption varies with the dielectric constant of the material. The electric dipoles present in the dielectric materials respond to the applied electric field of microwave. Resistive heating occurs when the dipolar orientation is unable to respond to the applied microwave field resulting into a phase lag.

Table 2.4 Microwave-Active Elements, Natural Minerals, and Compounds[50]

Element/ mineral/ compound	Time (min) of microwave exposure	T, (K)	Element/ mineral/ compound	Time (min) of microwave exposure	T, (K)
Al	6	850	NiO	6.25	1,578
C (amorphous, < 1μm)	1	1,556	V_2O_5	11	987
C (graphite, 200 mesh)	6	1,053	WO_3	6	1543
C (graphite, < 1μm)	1.75	1,346	Ag_2S	5.25	925
Co	3	970	Cu_2S (chalcocite)	7	1,019
Fe	7	1,041	$CuFeS_2$ (chalcopyrite)	1	1,193
Mo	4	933	$Fe_{1-x}S$ (Phyrrhotite)	1.75	1,159
V	1	830	FeS_2 (pyrite)	6.75	1,292
W	6.25	963	MoS_2	7	1,379
Zn	3	854	PbS	1.25	1,297

Table 2.4 (Continued)

Element/ mineral/ compound	Time (min) of microwave exposure	T, K	Element/ mineral/ compound	Time (min) of microwave exposure	T, (K)
Fe	7	1041	$CuFeS_2$ (chalcopyrite)	1	1193
Mo	4	933	$Fe_{1-x}S$ (Phyrrhotite)	1.75	1159
V	1	830	FeS_2 (pyrite)	6.75	1292
W	6.25	963	MoS_2	7	1379
Zn	3	854	PbS	1.25	1297
TiB_2	7	1116	PbS (galena)	7	956
Co_2O_3	3	1563	CuBr	11	995
CuO	6.25	1285	CuCl	13	892
Fe_3O_4 (magnetic)	2.75	1531	$ZnBr_2$	7	847

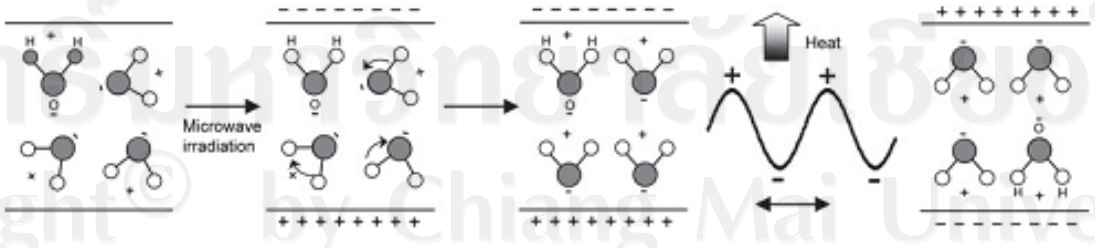

Figure 2.7 Heating mechanism of water due to microwave field[52].

2.3 Microwave plasma

At the pressures of $l0^{-3}$-10 Torr used for MW plasma processing, the average energy of the electrons is much higher than that of ions and neutral species, The excitation and ionization of atoms and molecules are thus essentially provided by electron impact on these heavy species. This implies that the shape of the electron energy distribution function (EEDF), $F_0(u)$, plays a major role in the density distribution of the various excited states of atoms and molecules, and in determining the ion density (n), for a given power density (PA) deposited in the plasma [53]. This is outlined succinctly in the following subsections.

2.3.1 Power transfer to the plasma

1). Power absorbed from the field per electron, θ_A, - In MW discharges, the operating frequency $f = \omega/2\pi$ is sufficiently high that the massive ions do not respond to the time-varying EM field; only the electrons are able to absorb energy from the field. In a DC discharge, an electron is accelerated continuously by the applied electric field (E) until it collides with another plasma constituent. The situation is totally different in high frequency (HF) discharges (which include both RF and MW cases): an electron is accelerated by the force F = -eE (-e is the electronic charge) in one direction during the first half of the period, and in the opposite direction during the second half. Averaged over one period, no net work is done and no energy is gained by the electron. It is only when this harmonic motion is interrupted by a collision that there is a net transfer of energy to the electron, which corresponds to the energy absorbed over the uncompleted period.

To characterize this power transfer, it is now customary to introduce the parameter θ_A as the power absorbed from the field per electron. Consider the plasma as being composed of a single fluid, the electrons (ions and neutral species being at rest), and neglect for simplicity the electrons thermal motion (cold plasma approximation). The equation of motion is then

$$m_e \frac{dv}{dt} = -eE - m_e \vartheta_c v \tag{2.7}$$

where m_e, is the electron mass and ϑ_c is the average (effective) electron-neutral collision frequency for momentum transfer. Since we assume a cold plasma, the electron velocity is fully governed by the electric field $E = E_0 exp^{(i\omega t)}$; thus from (2.14),

$$v = \frac{-eE}{m_e(i\omega + \vartheta_c)} \tag{2.8}$$

Since the work done by the electron per unit time is $F \cdot v$, we obtain, from its average over one HF perid,

$$\theta_A = \overline{-eE \cdot v(t)} = \frac{e}{2} Re(E \cdot v) = \frac{e^2}{m_e} \frac{\vartheta_c}{\vartheta^2 + \omega^2} \overline{E^2} \tag{2.9}$$

where Re means "the real part of", and the mean square value $\overline{E^2} = {E_0}^2/2$ We confirm that $\theta_A = 0$ when $\vartheta_c = 0$

2). Power loss per electron to the plasma, e, and power balance - Electrons transfer the energy acquired from the field to the plasma through collisions with heavy particles. The power loss on the average per electron in such collisions is given by [46]

$$\theta_L = \frac{2m_e}{M} < \vartheta_m(u) u > + \sum_j < \vartheta_j(u) > eV_j + < \vartheta_i(u) > eV_i \tag{2.10}$$

where M is the atom (molecule) mass, ϑ_m is the electron-neutral collision frequency for momentum transfer for an electron of microscopic energy u, and, V_j and V_i, are the electron collision frequencies leading to excited atomic (molecular) species "j", and to ionization, respectively; eV_j and eV_i, respectively, are the corresponding energy thresholds for excitation and ionization. The bracket < > means the average value over the EEDF.

Charged particles can "leave" the plasma by ion-electron recombination, either in the plasma bulk (volume recombination), or as a result of diffusion to the discharge vessel wall. When the electron density is not too high (typically $n \leq 10^{12}$ cm^{-3}) and the average energy is not too small ($\langle u \rangle \geq$ l ev, one can assume that the charged particles are lost by diffusion to the wall [48]. In this case, provided that atoms (molecules) are excited and ionized by single electron impact events from the ground state, <u> (or the electron temperature T_e, if the EEDF is Maxwellian) and θ_L, can be assumed, as a first order approximation, to depend only on the discharge conditions (discharge vessel dimensions and shape, nature and pressure of the gas, frequency, and static magnetic field intensity), whatever the microwave power density absorbed in the discharge.

Under steady-state conditions, the power absorbed from the field adjusts to compensate for the loss of electron energy to the plasma, yielding the power balance equation

$$\theta_A = \theta_L \qquad (2.11)$$

2.3.2Microwave plasma application for materials synthesis

Microwave-induce plasmas have always enjoyed a distinct place in the literature. In 1964, McTaggart [54] wrote extensively about MW plasmas. After that, Wightman [55] reviewed article entitled "Chemical Effects of Microwave Discharges" which surveyed the literature from 1965 to 1973, made the statement that "there is sufficient evidence to indicate that chemical results obtained with the microwave plasma differ significantly from other plasmas". Two further review papers on the subject by Lebedev and Polak [56], and by Musil [57] followed in 1979 and 1986, respectively; and finally, in 1992, two books edited by Moisan and Pelletier [58], and by Ferreira and Moisan [59].

There are many compounds has been studied via microwave plasma. In 1996, J. D. Houmes prepared recently a number of nitrides such as TiN, AlN, and GaN by the use of a plasma by exposing oxides to plasma of N_2/H_2 [60]. In the same year, R.E. Douthwaite had reported a rapid synthesis of alkali metal fullerides by using microwave induced argon plasma. Reaction times was reduced to only a few seconds while the conventional preparation takes a very long time. The microwave plasma was generated in argon held at a pressure of 10^{-5} mbar in evacuated quartz tubes. Fullerenes and alkali metals are kept physically separated, and the tube was at the position that the microwave amplitude was at the highest. The alkali metal quickly heated and vaporized, and the C_{60} reacted with condensed K under the Ar plasma. Under these conditions, K intercalated easily. It was also confirmed that uncondensed K in the plasma did not intercalate. It has been shown by alteration of reaction conditions that there is a thermal action of the plasma which is responsible for the rapid synthesis [61]. Afterwards in 1997, Binary (TiN, AlN, and VN) and ternary (Li_3FeN_2, Li_3TiN_2, Li_3AlN_2) nitrides were synthesized by microwave-assisted which

a direct reaction between metal powder and nitrogen by first striking a N_2 plasma.

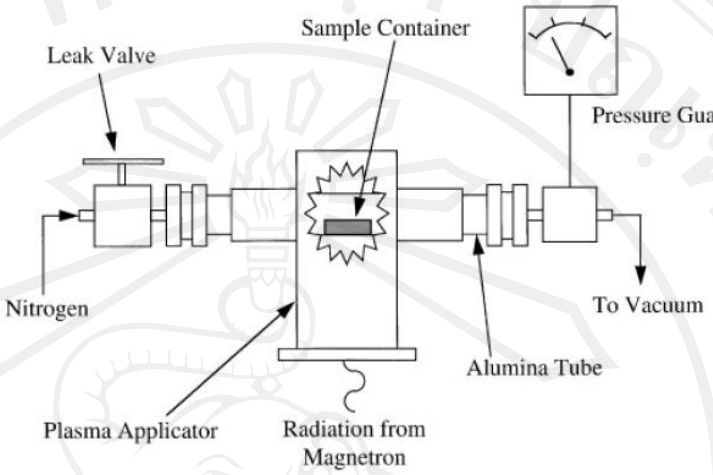

Figure 2.8 Schematic diagram of Cober microwave system used in the synthesis of binary nitride materials by reaction with a nitrogen plasma.

Homogeneous microwave plasmas have been produced and used for materials surface modification was presented Wu[62]. In 2000, the results of new 160-mm homogeneous plasmas produced at the pressure of 10-600 Pa. Also, the axial distributions of plasma parameters have been investigated, with and without the short circuit at the top of the setup, respectively. The experimental results showed that the short circuit was efficient for the plasma density being raised and beneficial for plasma uniformity. Beside these, nitrogen doping into titanium dioxide (TiO_2) nanoparticles have directly synthesized in atmosphere of microwave plasma-torch using gas-phase titanium tetrachloride ($TiCl_4$) [63]. Microwave plasma torch system was presented for perform in the low pressure chamber to make continuously sustained plasma. The plasma density increases as the microwave power increase. Disintegration of nitrogen fluoride (NF_3) indicates that a microwave plasma torch operating at a low pressure can efficiently generate an abundant amount of chemical radicals [64].

Continuous wave (CW) microwave discharges was presented to operate at atmospheric pressure in argon gas were applied to surface modification of metal surfaces for improvement of adhesion with coating as shown in Figure 2.9. For the basis of application, the charged particles in the discharge plasma with high kinetic energy bombard the substrate, cleaning and etching its surface in rough morphology and polluted with organic compounds as shown in Figure 2.10 [65].

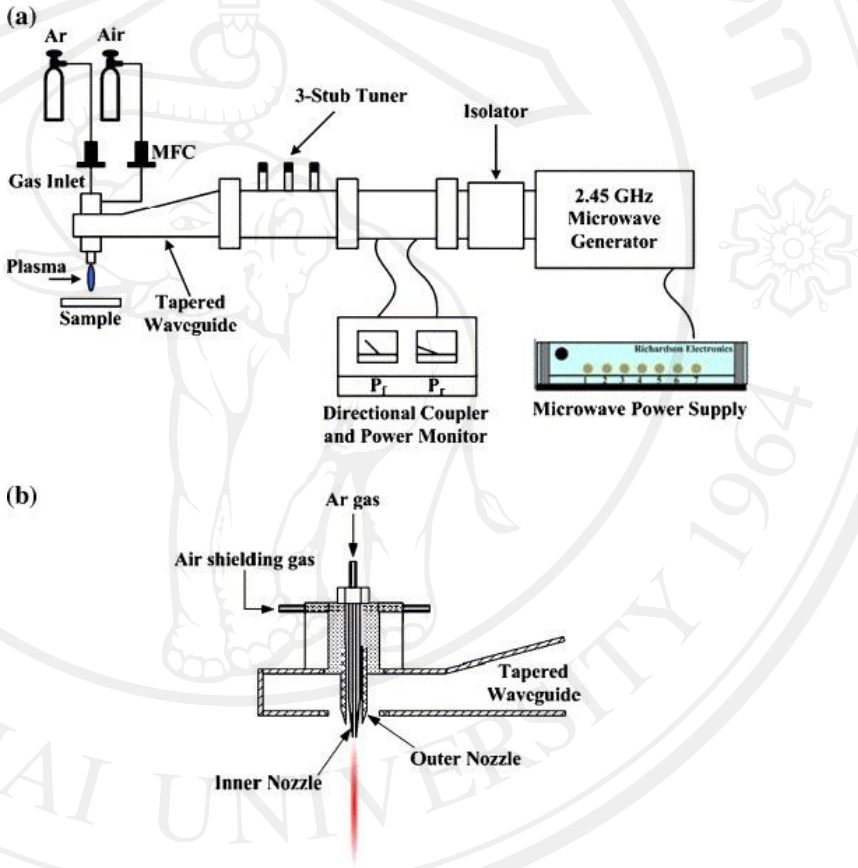

Figure 2.9 Schematic diagram of (a) the apparatus for plasma modification by making use of an atmospheric microwave plasma torch and (b) the construction of the plasma nozzles.

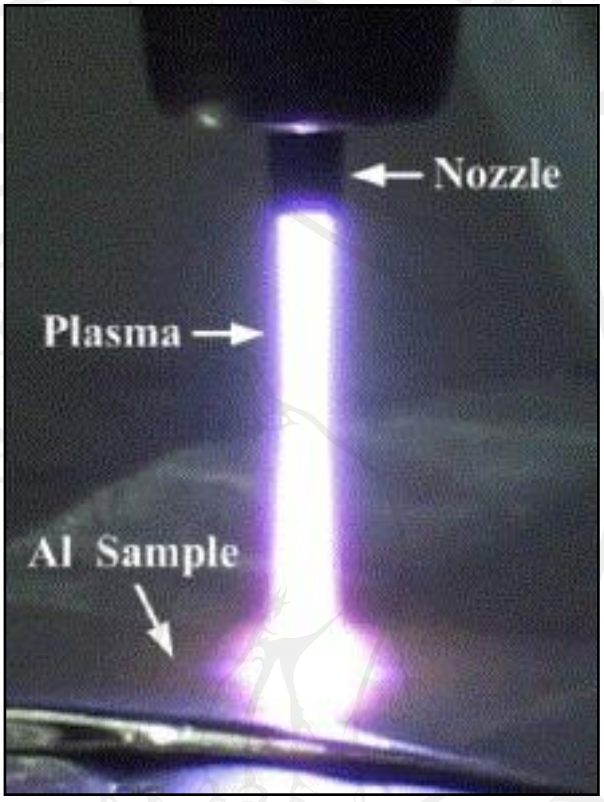

Figure 2.10 A photograph of the microwave plasma in operation for the treatment of Al sample.

Easily binary composition oxide synthesize was reported by Y. C. Hong. Mg granules were fill in torch flame of an oxygen microwave plasma. The plasma torch vaporized Mg granules immediately and then, vapor became to form MgO nanopowder as following mechanism of oxidation (Figure 2.11) [66].

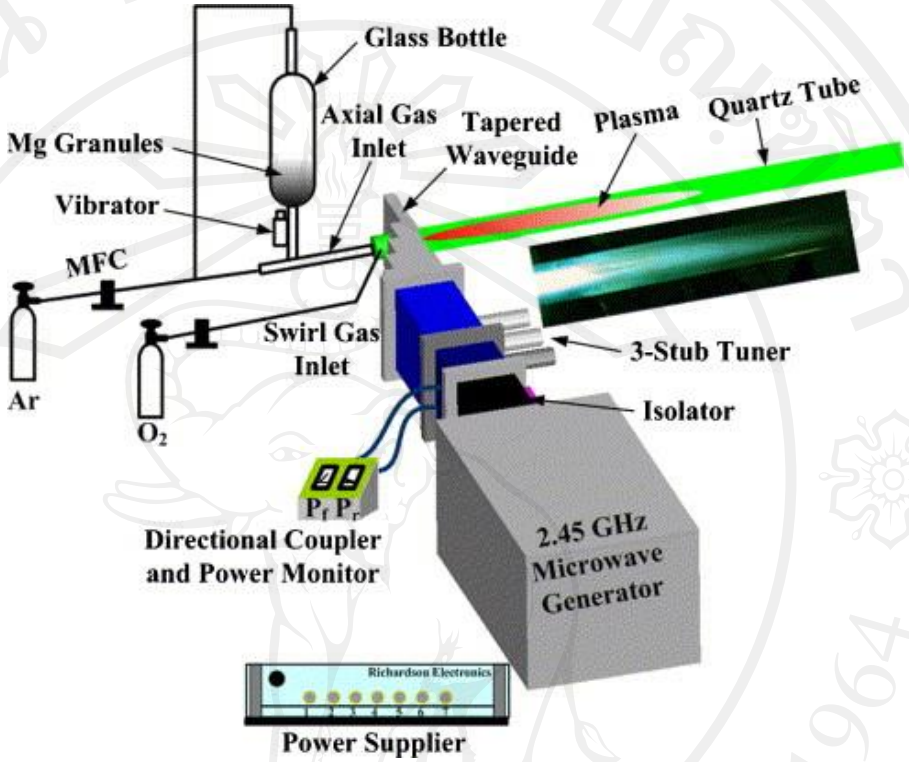

Figure 2.11 Schematic presentation of the synthetic system of MgO nanoparticles with the atmospheric microwave plasma torch. The inset shows the plasma emission of green color after completion of the synthesis.

Sintering of complex solid oxide had also been reported in 2007 by Q. Zhen [67]. Nanocrystalline of Bi_2O_3-HfO_2-Y_2O_3 samples were sintered in microwave plasma at 700ºC for 30 min, the relative density was found to the greater than 96%. Moreover, the sintered specimens exhibit considerably finer microstructure and greater densification, compared with sintered sample from conventional method Figure 2.12.

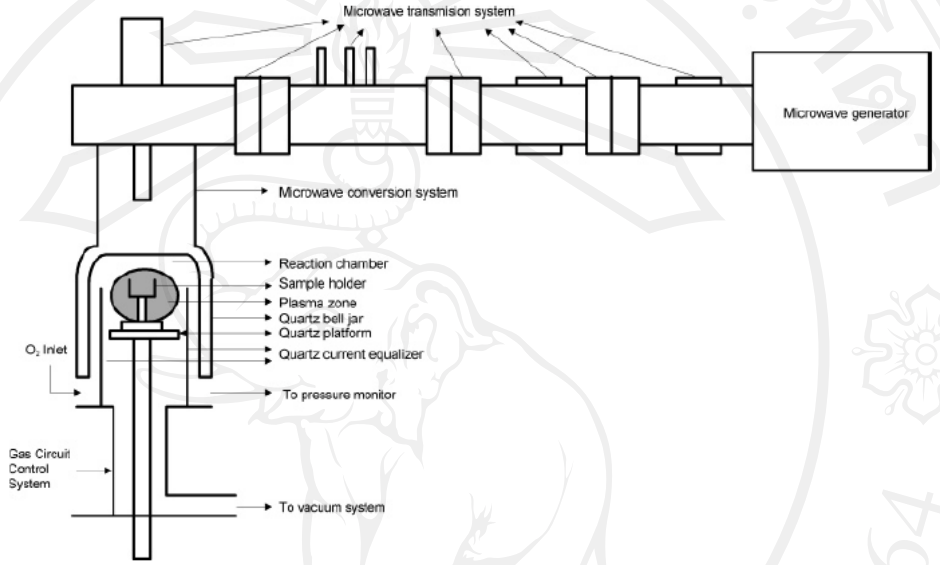

Figure 2.12 A schematic diagram of microwave plasma equipment.

2.4 DC electrical heating

2.4.1 Direct current heating method

This technique is a high efficiency route for materials synthesis and processing. It makes possible synthesis and sintering at low pressure surrounding and short periods by charging the intervals between powder particles with direct electrical current (DC) energy and effectively applying at high temperatures. It is regarded as a rapid processing method with the uniform heating.

2.4.2 Basic configuration of the system

Figure 2.13 shows the basic configuration of the direct electrical current heating system. The system consists of a vacuum/argon-gas atmosphere control chamber with a vertical uniaxial pressurization mechanism of electrodes which be placed on top and bottom of the powder which is in mold. For operate the system, the chamber will be evacuated to vacuum condition or prepared as gas rich atmosphere. Then, DC current will be directly apply through powder for heat up the system. Meanwhile, the pressurization mechanism press on the powder.

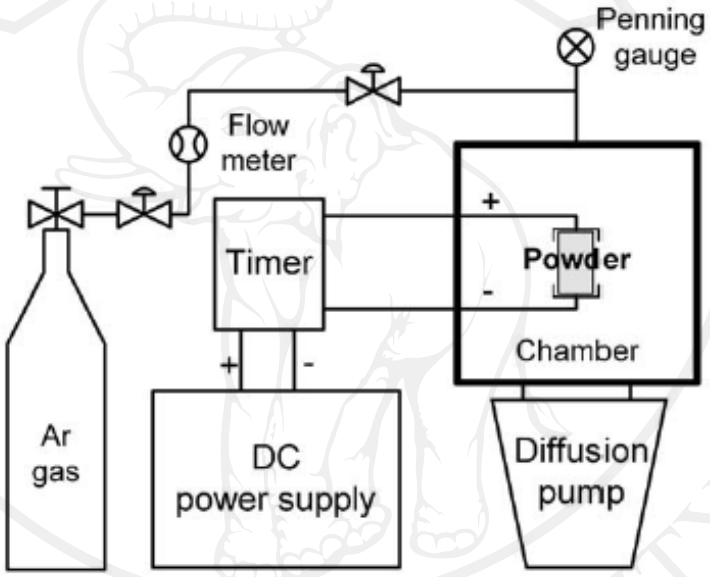

Figure 2.13 A schematic diagram of direct current heating method apparatus[68]

2.4.3 DC pulse current energizing effect

The DC energizing method generates[69]: (1) spark plasma, (2) spark impact pressure, (3) Joule heating, and (4) an electrical field diffusion effect. In the process, the powder particle surfaces are more easily purified and activated than in the conventional processes. Material transfers at both the micro and macro levels are promoted. So, a high-quality synthesized and sintered compact is obtained at a lower temperature and in

a shorter time than with conventional processes. Figure 2.14 illustrates current flows through powder particles.

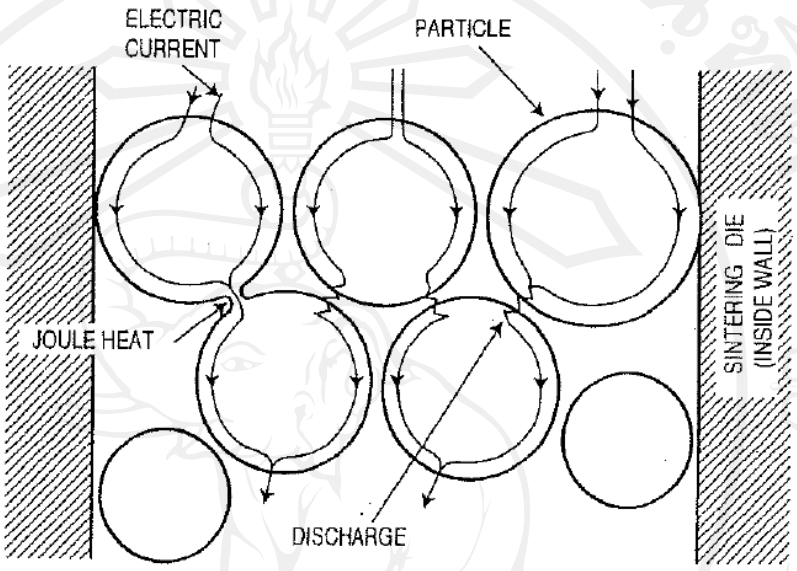

Figure 2.14 Pulsed current flow through powder particles [69]

2.4.4 Synthesis by using direct electrical current heating method

There are many researcher studied about materials synthesis and processing by using direct electrical current heating method and related techniques. In 1999, N. Abdenouri et al.[70] had presented about using Transferred-arc plasma treatment iron sulfides containing gold. In the process had varied plasma gas source: argon plasma with sulfide, argon plasma with a carbon-sulfide mixture, and argon me thane plasma with sulfide. The reduction with a Ar-CH_4 (10%) plasma is a proved alternative process process. A gold extraction efficiency of 90% is achieved for batchs melting operations. After that, Y. Makino (2003) [71] had synthesized by using pulsed high current heating (PHC). In this method, the powder in a graphite die is pressed uniaxially and then a pulsed direct current is applied. The current generates a spark discharge between particles. The crystallite size of the anatase

densified using the PHC heating method gently increased from 10 nm (in the starting powder) up to 43 nm, with increasing relative density. While the size of the conventionally-densified anatase rapidly increased to over 50 nm irrespective of relative density.

P. Singjai (2007) [72] presented that the Large-scale production for ZnO nanowires had been produced by current heating deposition. Based on the use of a solid–vapor phase carbothermal sublimation technique, a ZnO–graphite mixed rod was placed between two copper bars and gradually heated by passing current through it under constant flowing of argon gas at atmospheric pressure. The product seen as white wool deposited at the rod surface which was separated for further characterizations. The results have shown mainly comb-like structures of ZnO nanowires in diameter ranging from 50 to 200 nm and length up to several tens micrometers. From optical testing, ionoluminescence spectra of as-grown and annealed samples have shown high green emission intensities centered at 510 nm. In contrast, the small UV peak centered at 390 nm was observed clearly in the as-grown sample which almost disappeared after the annealing treatment.

S. Thongtem (2009)[73] had produced CuS (hcp) with different morphologies by using a transient solid-state reaction by the direct flow of electricity through solids, containing 1:1 molar ratio of Cu:S powders, in a high vacuum system for different lengths of time. A 20 A of direct current was applied to prepared powder on 1,3,5 second and 3 minutes processing time, respectively. The results shown a better crystallinity in a longer operating time condition.

2.5 Gas sensor based on metal oxide semiconductor

Semiconducting Metal Oxide (MOS) gas sensors are advanced sensor types. Since the pioneering reports on their gas sensitivity at elevated temperatures in the 1950s [74], gas sensors based on these MOS for detection of hazardous,

flammable, and toxic gases has been increasingly developed because of their small dimension, low cost, and high compatibility with microelectronic processing [75-77]. The physical and chemical properties of nanoscale materials are strongly influenced by their dimensional constraints and morphologies. Gas sensors based on nanostructured MOS are expected to exhibit better performance than their bulk or microcounterparts. In this regard, metals oxide nanostructures, such as 1D nanowires, 1D nanorods, 2D nanosheets, 3D nanoflowers, and complex hierarchical architectures, have attracted considerable interest for their potential as building blocks for fabricating gas sensors because of their high effective surface areas [74–77].

Firstly, the oxide surface is absorbed by oxygen atom when the system is exposed to air. At lower temperatures, the surface reactions are very slow to be useful comparison with at higher temperature. The adsorption of oxygen species ,O^-_2, O^- and O^{2-}, has acquired electrons from the conduction band. The adsorption kinematics are explained by the following reaction paths [78-79]:

$$O_2(gas) \leftrightarrow O_2(absorbed) \quad (2.12)$$

$$O_2(absorbed) + e^- \leftrightarrow O_2^- \quad (2.13)$$

$$O_2^- + e^- \leftrightarrow 2O^- \quad (2.14)$$

$$O^- + e^- \leftrightarrow O^{2-} \quad (2.15)$$

The oxygen species of O^-_2, O^- and O^{2-} are stable when the oxygen ions are at temperature below 100 ◦C, in range of 100 to 300 ◦C and at above 300 ◦C, respectively. The electrons in the conduction band of n-type MOS are removed by the adsorbed oxygen ions. According to this phenomena as showing in Figure 2.15 and 2.16, the electron concentration at the oxide surface decrease. For n-type MOS sensor, majority carriers are electron, the resistance of n-type MOS sensor decreases when the temperature increases due to their semiconducting properties. However under oxygen atmosphere, This causes a decrease of the carrier concentration and an increase of resistance of n-type MOS sensor at operating temperature. When the n-type MOS sensor is under the reducing gas ambient,

the electrons released from the chemical reaction are given back to the conduction band leading to a decrease of the sensor resistance. In the other hand, the majority carriers in p-type MOS are holes. Similar to n-type MOS, the sensor resistance of p-type MOS decreases when the temperature increases. However, under oxygen ambient, p-type MOS generates holes when the oxygen ions are adsorbed on the surface via the excited electrons from valence band. This process results in raising the number of charge carriers, which leads to a decrease of the sensor resistance (opposite to n-type). When the p-type MOS sensor is under the reducing gas ambient, the electrons inject into the valence band and recombine with the holes and this method resulting in reducing the number of holes, which leads to an increase of the sensor resistance.

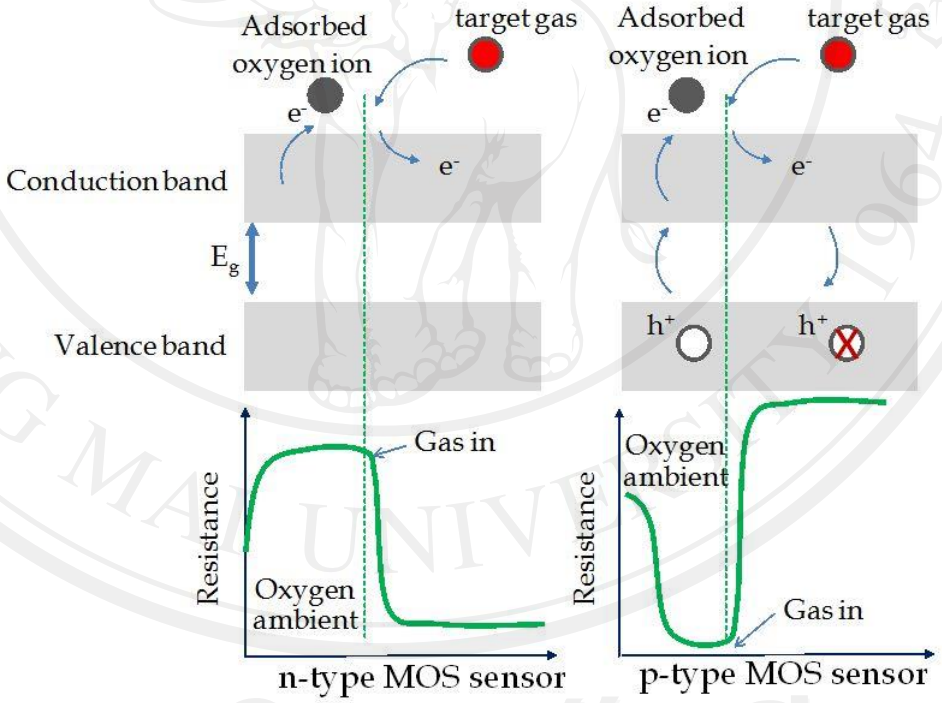

Figure 2.15 Schematic diagram for change of the sensor resistance upon exposure to the reducing gas in the cases of n-type and p-type MOS sensors [80]

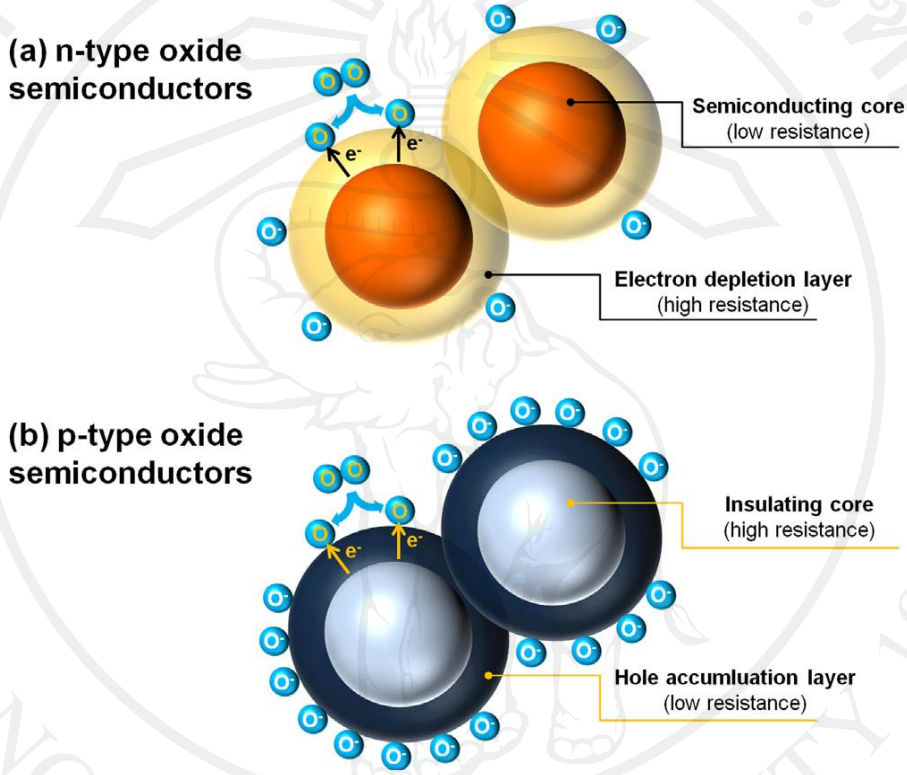

Figure 2.16 Formation of electronic core–shell structures in (a) n-type and (b) p-type oxide semiconductors [81]

the gas-sensing response for n-type semiconducting oxide to reducing is defined by following equation:

$$S = R_a/R_{rg} \quad (2.16)$$

In case of p-type, the response for p-type semiconducting oxide to reducing gas has a relation as shown in below:

$$S = R_{rg}/R_a \quad (2.17)$$

where R_{rg} and R_a are the electrical resistances of the sensors measured in the presence of reducing gas and pure dry air, respectively.

In addition to the importance term of gas response, the gas-sensing characteristics of MOS sensor can be characterized by response and recovery times. The response time, T_{res} is typically defined as the time required to reach 90% of the steady response signal while the recovery times, T_{rec} is denotes as the time needed to recover 90% of the original baseline resistance [82]. However, only response value is considered for general comparison of different reports in the following section because it is derived from steady-state values while response or recovery time obtained from different works are not comparable because of different gas flow configurations.